Chapter 3

Microstructural and magnetic characterization technics

3.1 Optical Microscopy

The samples studied in this work, due to their ceramic character, present a microstructure with a lot of defects. Besides, the presence of Ag as welding agent in the superconducting joints and the high temperature welding process, can change the microstructure near by the joint area.

This work focuses on a detailed study of the microstructure of the superconducting joints. One of the techniques used for analysis is the optical microscopy (MO) with polarized light.

The use of this technique is based on the observation of polished surfaces in polarized light. The surfaces to be characterized must be previously prepared. The surfaces are polished using SiC abrasive disks with different particle size down to 300μm. We have used water as lubricant for the polishing process. The H_2O affects superficially the YBCO material, forming carbonates and if it is used for long time can destroy the sample. Thus, it is important to minimize its use. When this step is finished, the surfaces are polished using diamond disks with particle size of 9, 6, 3 and 1μm, respectively. In this case we have used some special lubricant based on ethanol which does not damage the sample.

The polished surface is then analyzed by using a NIKON LABOPHOT micro-

scope. The microstructure observed in this way is captured by means of a digital camera. When relatively non-superconducting phases, like $BaCuO_2$, Y_2BaCuO_5 phases and Ag precipitates in the big amount in the YBCO matrix, are formed at the YBCO/Ag/YBCO interface they can be easily detected by this technique. Unfortunately, the Ag precipitates cannot be detected if they are small. For this, SEM microscopy with EDX and WDS analysis have been employed to detected it.

3.2 Scanning Electron Microscopy (SEM)

Another technique used to characterize the microstructure of the samples studied in this work is Scanning Electron Microscopy (SEM). It is considered the most useful technique to visualize and analyze the microstructure of solid samples, basically due to its high resolution (about 3.5nm) and its large depth of field, which allows a large amount of the sample to be in focus at one time. Using SEM, the most common defects found in the superconducting materials such as: microcracks, macrocracks, grain misalignment, porosity, etc. can be observed. Additionally, different phases formed in the YBCO matrix during the high temperature welding process and the distance to which Ag has migrated into the solid YBCO can be detected.

To obtain a good microstructural characterization, a previous preparation of the superconducting joints is necessary. Thus, we have used the same steps of polishing which have been followed when an optical observation has been performed. Additionally, for a better visualization of the microstructure of the samples studied in this thesis, we have used a chemical etching to the superconducting YBCO matrix. During the polishing process, the microcracks existent in the sample could be filled-up with fine particles created during this process. Thus, one of the purposes of this etching is to visualize better the orientation of the microcracks or macrocracks existent. The angle between the microcracks existent in both monoliths gives us the disorientation of the monoliths. For in-

stance, the sample is etched for 60 seconds in acetic acid, 10% diluted, and, after, cleaned using ethanol.

This study has been done by using a JEOL microscope, type JSM-840 and with a maximum magnification of x300 000 provided by Servei of Universidad Autonoma de Barcelona. The scheme of this microscope is shown in figure 4.1. This microscope has incorporated three components:

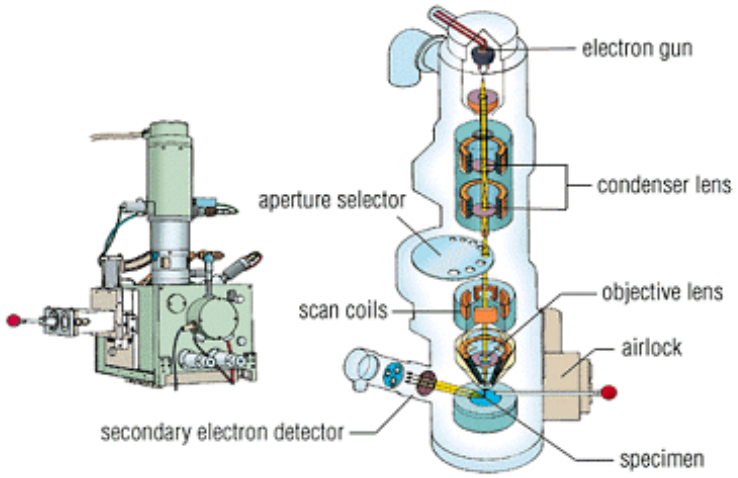

Figure 3.1: Scheme of Scanning Electronic Microscope

1. Microanalysis probe with Energy Dispersive X-Ray (EDX, Oxford Instruments ISIS 200) which allows both, qualitative and semiquantitative identifications of the chemical elements existing in the sample. Also, allows to observe the distribution of these elements on the polished surfaces;

2. Secondary Electron Imaging (SEI) which is a detector with secondary electrons allowing to obtain images with high resolution. The secondary electrons are all those electrons emitted by the sample, not those which penetrate the material and their energy is low, under 50eV;

3. Backscattering Electron Imaging (BSE) which is a detector with dispersed electrons allowing to observe the composition and the topography of the

surface. The energy of the dispersed electrons is higher. By using this component, we can obtain an image of the microstructure of the surface, giving a compositional contrast because of the different elements existent in the sample which have different atomic number and which emit signals with different intensities. The difference between both electrons is only the energy which is emitted by the sample.

Once etched, the sample is situated in a support using Ag paint and introduced in the vacuum chamber of the microscope for analysis.

Using EDX we have detected the segregation formed during the welding process, the carbonates that damage the superconducting properties of the samples and the Ag particles, which have a different aspect according to the technique used. As well, we have determined the distance to which the Ag penetrates into the YBCO matrix which is critical for the optimization of the welding process.

Using SEI we have observed the porosity and the microcracks existing in the polished surfaces. The misalignment of the single domains can be detected by observing the misalignment of the micro and macrocracks of the final joint in both single domains which were joined.

3.3 Electron microprobe analysis

To determine the elemental composition of the YBCO/Ag/YBCO interfaces and to quantify the Ag into YBCO solid we have used a Cameca SX-50 microprobe equipped with four Wave Dispersive Spectrometers (WDS) and one Electron Dispersive Spectrometer (EDS) from Servei of Universitat de Barcelona. This instrument allows elemental analysis of all elements of atomic number 4 (boron) or greater. Detection limits are of order of 100ppm (by weight) and the samples can be viewed optically by transmitted or reflected light and the images stored digitally.

Detection limit is commonly understood to be the smallest concentration we can measure with a particular technique. In fact it is the point at which we

can make a decision whether the element or compound is present or not in the sample.

The characteristic X-ray spectrum is superimposed on a background of "white" radiation in which all wavelengths are represented. The background, measured at a convenient offset from the peak position, is subtracted from the peak height. The background position must also be chosen so as not to overlap the peak for some other element which may occur in the specimen.

The net intensity of the characteristic X-ray peak is proportional to the mass concentration of this element in the sample. However, quantitative analysis relies on comparing the sample analyzed with a standard of known concentration of the element. The standards are calibrated in a separate session to establish the net counts per unit concentration for each element. In our study, the calibration of the microprobe was performed with high purity standard yttrium, barium, copper and silver. We performed analysis in the molten region YBCO/Ag/YBCO of the quenched samples and in the YBCO matrix to observe the extension of Ag penetration.

The detection limit of the microprobe (3.1) is determined as follows:

$$LD = \left[\frac{C^S}{(I_p^S - I_f^S)}\right] \times 3\sqrt{2} \times \left(\frac{I_f}{t_f}\right)^{1/2} \tag{3.1}$$

where

- LD is the detection limit (wt%);
- I_p^S is the peak intensity measured on the reference sample (c/s);
- I_f^S is the peak intensity measured on the reference background (c/s);
- I_f is the peak intensity measured on the background (c/s);
- t_f is the peak time measured on the background (s);
- C^S is the concentration on the reference sample (wt%);

As the microprobe focuses on a small micron sized area, the sample should be prepared previously. The preparation consists of polishing the analyzed surface using SiC and diamond disks down to 1μm particle size.

For our experiments we have used a voltage of 20keV, a current beam of 100nA and a 10 seconds count time to obtain the required accuracy of better than 1%. According to these equations, the detection limit calculated was 0.016at%.

3.4 Scanning In-field Hall Probe imaging system

The properties of the superconducting materials, especially the critical current density, are usually determined through magnetic measurements. Methods like dc magnetometry lead to an understanding of global properties of these materials such as: magnetization, magnetic susceptibility or critical currents. However, to observe the relation between microstructure and superconducting properties a local analysis of these materials is necessary. These studies can be done by means of magneto-optics at reduce magnetic fields and Scanning Hall Probe imaging which can use very high magnetic fields. In this PhD thesis the Scanning Hall probe imaging has been used for the characterization of the welded samples.

3.4.1 Principle

The Hall Probe method is based on the Hall effect discovered by E. H. Hall (1897). According to this theory, if an electric field flows through a conductor in the presence of a magnetic field, the magnetic field exerts a transverse force on the moving of charge carriers which tends to push them to one side of the conductor. A build up of charges at the sides of the conductor produces a voltage between the two sides of the conductor. The voltage produced is called Hall

voltage (V_H) and is defined as:

$$V_H = R_H \frac{BI}{d} \tag{3.2}$$

where d is the thickness of the sample and R_H is the Hall constant, B is the magnetic induction and I is the applied current.

A Hall Probe can be a small piece of semiconductor. Four leads are connected to the middle points an opposite sides. If a constant current is applied, the Hall voltage is directly proportional to the induction.

The sensitivity of the probe is defined by the ratio:

$$\frac{R_H}{d} \tag{3.3}$$

where d is the thickness of the semiconductor layer and R_H is the Hall resistance.

3.4.2 Hall probe set-up

Scanning Hall Probe imaging is influenced by external parameters such as the active surface of the probe and the distance between the sample and the probe.

For the superconducting characterization of the samples obtained by the joining method we have used an AsGa Hall Probe with an active area of 0.1x0.1 mm^2. The strong dependence with the distance from the surface of the sample of the magnetic induction generated by the sample, requires scanning the probe at the smallest distance as possible.

Thus, in the Hall system used in this thesis, the distance between the sample and the semiconductor layer is about 80μm. If the semiconductor layer is in contact with the sample, the first one could be damaged. A small distance must exist in order to protect the probe. The system field noise was measured to be smaller than 4 $\cdot 10^{-5}$ T (at 2 $\cdot 10^{-3}$ Hz).

The probe is located above the sample and glued in the arm (glass reinforced epoxy) used to raster it over the polished surface of the sample. The Hall measuring system is located in a dewar placed between the two poles of an electromagnet, which allows applying an homogeneous magnetic field H perpendicular to the sample surface, ranging from -1 to 1T [29].

One can either follow a field-cooled process (fc) under the maximum available field, in order to determine the remanent magnetization or apply a zero-field cooled process (zfc) and measure successive maps at different applied fields.

3.4.3 Scanning imaging set-up

Field mapping is done by scanning the Hall probe on an x-y sledge in steps of dx=dy=160μm. A scheme of this experimental set-up is shown in figure 4.2 left.

As it can be seen in this figure, the sample is located in an aluminium support and fixed with vacuum grease to avoid sample movements during the measurement. The Hall Probe is rastered above the sample by using the glass reinforced epoxy arm. The movement of the probe is controlled by two motors: one for the transverse movement (motor y) and the other one for the longitudinal movement (motor x). The motors are controlled by a computer and the pick-up signal is connected by an amplifier to 12 bits analogical digital converter. The distance swept in the longitudinal direction is controlled by two sensors and in the transversal direction by a computer program. In this way we can fix the zero scanning position and the length of the surface sample, thus the probe sweeps all the surface sample.

A liquid nitrogen dewar is located between the two poles of an electromagnet (see figure 4.2 right). The system sample-support-probe is situated inside the dewar so that the sample is in the center of the electromagnet where the magnetic field is homogneous.

The control of the sample position is very useful to analyze the results of field mapping experiments. This helps us to obtain a relation between the mi-

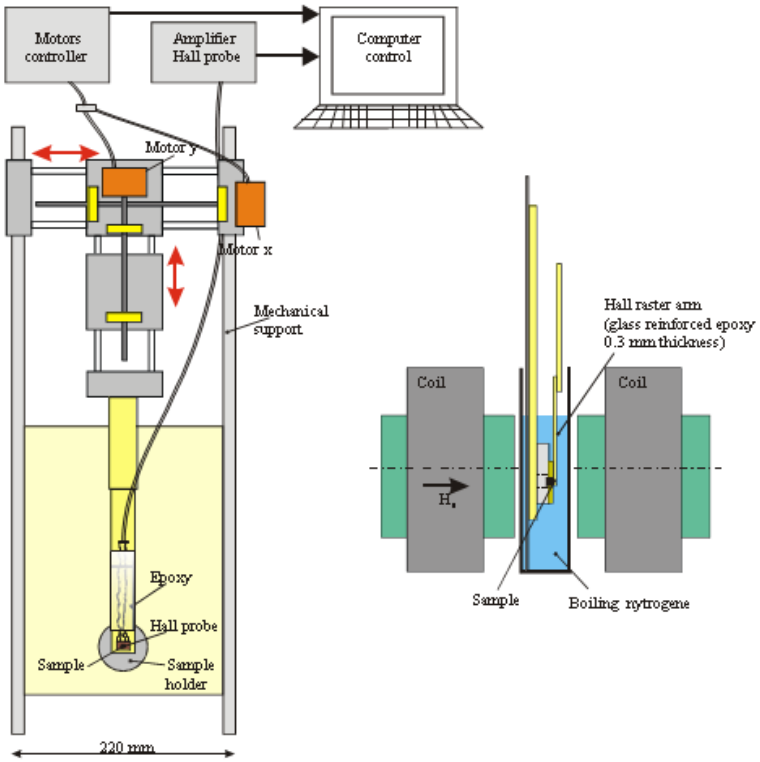

Figure 3.2: Scanning Hall Probe imaging set-up

crostructure and the superconducting properties of the sample. Thus, a mark is made on the sample at the side where the scanning has started.

3.4.4 Trapped field measurements

As it has been mentioned, an important property that must fulfil a superconductor to be used in technological applications is to trap high magnetic fields.

The magnetic field trapped by a superconductor can be determined in a field-cooled process. This method consists of cooling down the sample below its critical temperature, T_c, in the presence of an external magnetic field. When the sample reaches this temperature, the external magnetic field is removed from the sample. Soon after, the scanning of the surface sample starts and the magnetic field trapped in each point by the sample is measured by the Hall Probe. It

is a rapid and non-destructive way to characterize the samples.

3.4.5 Estimation of critical current density

The trapped magnetic field is not a good enough physical magnitude to characterize the welding quality and compare different samples since it depends on the sample size and shape (see Chapter 2). The determination of the critical current density of the samples allows this drawback to be overcome and characterizes the amount of current that crosses the joint.

For small samples it is easier to determine this magnitude by measuring the magnetization using SQUID or PPMS devices. Unfortunately, for big samples the use of these devices is impossible so a method to determine the critical current density from the Hall Probe measurements is needed. M. Carrera *et al.* [30] have given solution to the inverse problem. As a consequence, they have developed a software called "Caragol" and which can be found on-line on "http://jaumetor.upc.es/caragol/". The starting point of the computation is a superconducting sample AxI, which is a straight cylinder over a base A of arbitrary geometry; I is the height of the cylinder. In this algorithm it is assumed that:

1. the current circulation is planar (i.e. confined in the basal plane);
2. the planar current in every vertical section is the same; i.e. the current is constant in the z direction (no demagnetizing effects are considered though they have been shown to not be important in samples of several mm like the ones analyzed in this thesis [31]).
3. the field dependence on z direction is considered.

The originality of this method is that it does not require any geometric assumption of the planar current. Thus, the algorithm may detect the existence of in-plane irregular current distributions which is very useful to detect sample inhomogeneities.

The computation starts from the magnetic field profile determined by Hall probe measurements. The sample and its neighborhood are divided in a fine rectangular mesh, henceforth called the discretization lattice and it is assumed that the magnetization M has a constant value M(i,j) in every rectangle of the matrix. Therefore,

$$B_z(x_m, y_m, h) = \sum_{i,j} M(i,j) \cdot \frac{\mu_0}{4\pi} \int_{\Delta ijxI} \frac{3z^2 - r^2}{r^5} dxdydz \tag{3.4}$$

This equation 3.4 represents the interpoled Biot-Savart equation and depends only on the geometry of the problem. Equation 3.4 becomes a set of linear equations on the unknowns M(i,j) and, using the measured B_z over a mesh of points (x_m, y_m, h), a determined linear system of equations can be constructed. Once the magnetization is determined, the current $J_{i,j}$=(J_x, J_y) can be calculated by computing $\nabla \times \overrightarrow{M}_{i,j}$.

Thus, to determine the critical current densities of the final joints obtained by the welding process, first we have measured the trapped field of the sample and after, by using the "Caragol" software described before we have determined the critical current density of both, the bulk and the final joint, simultaneously. The exact procedure for this simultaneous determination is described in Chapter 7.

To validate this method, a comparison of the measured magnetic field B_z with that induced by the calculated solution has been done. In figure 3.3 it is represented the measured and calculated B_z profile for a FC process obtained for a joint obtained by the welding process proposed by us. The joint is indicated in the figure by arrow. The $B_{measured}$ profile is indicated by the red line and the $B_{calculated}$ profile by the black line. The estimated error between both is about 5%.

3.4.6 Detection limit of the Hall probe imaging system

In order to determine the quality of the final joints and compare them with the original sample is important to know the detection limit of the probe. Detection limit is commonly understood to be the smallest value of the remanent

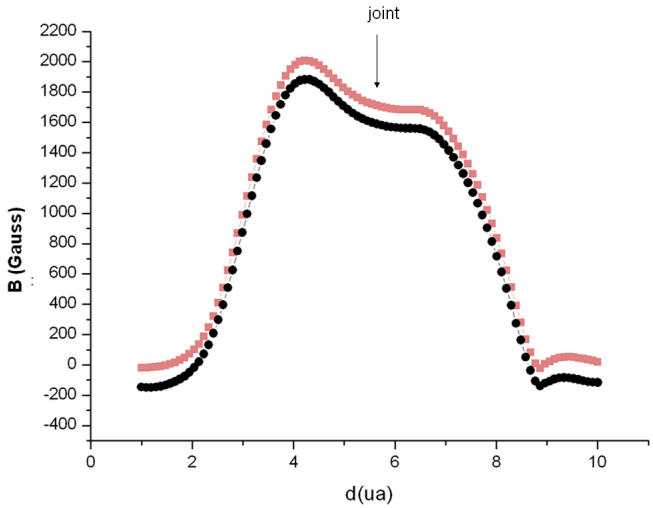

Figure 3.3: Comparison between the $B_{measured}$(■)- red line and $B_{calculated}$ (•)-black line for a joint obtained by the welding process. The junction is indicated in the figure by an arrow.

magnetization we can measure with this technique.

In this way a very simple experiment has been done. First we have measured the remanent magnetization after a fc process for an YBCO single domain. Afterwards, we have measured an artificial YBCO/YBCO joint obtained by simply gluing the both YBCO domains with loctite.

For instance, the simplest test available with the Hall system is the remanent magnetization (M_{rem}) map of the sample after following a fc process. First, the ab plane of a YBCO pellet previously oxygenated and with dimensions of about 1x1x0.6cm^3 is polished. An external magnetic field of $\simeq$ 5000Oe is applied to the sample and then the sample is cooled down to 77K. Once the YBCO pellet reached this temperature, the magnetic field is removed from the sample and the Hall probe is scanned over the ab surface.

Figure 3.4a shows the magnetization profile at the remanent state after a field cooled process of the YBCO pellet. The remanent magnetization in the center of the sample is of $M_{rem}\simeq$2400 Gauss. It can be observed that flux penetrates into the right part of the sample with a gradient lower than in the left part. This indicates that the remanent magnetization at the right part is slightly lower

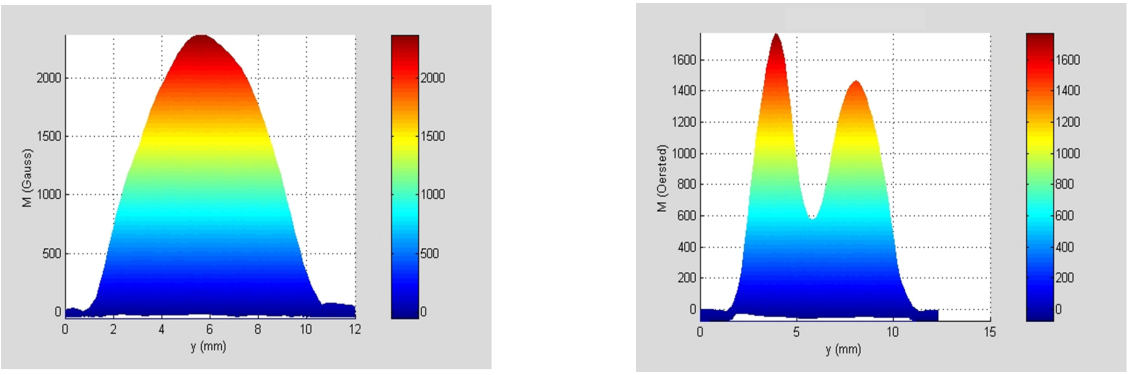

(a) (b)

Figure 3.4: In-field Hall microprobe remanent magnetization profile measurements of an YBCO sample with the applied magnetic field parallel to the [001] axis: Remanent magnetization profile after a field cooling process: a) original YBCO sample; b) glued sample.

then the one from the left-hand side. Thus, it is important to take into account that the starting sample present some inhomogeneities which can affect the properties of the final joint.

For comparison purposes, the YBCO sample is cut into two parts and the ac surfaces are glued. This can be considered as a case of completely non-superconducting joint. In figure 3.4b it is represented the remanent magnetization of the glued sample, after a field-cooled process in the same conditions as the original sample. Thus, an external magnetic field of $H_{applied}\simeq$5000 Oe is applied parallel to the c-axis of the sample and to the junction. This profile shows two clearly differentiated peaks. For instance, a totally non-superconducting joint can be detected by the Hall probe imaging system used in this thesis for the characterization of the YBCO/Ag/YBCO joints. The maximum remanent magnetization measured at junction is of $M_{rem}\simeq$600 Gauss and compared with the YBCO grain is reduced by 60-70%. Thus, any joint whose remanent magnetization measured with the present Hall imaging system, is reduced by 60-70% after the welding process could be considered to be non-superconducting. Additionally, as it could be observed in the original sample, the magnetization peak from the right-hand side has a lower value than the magnetization peak from

the left-hand side of the image.

Chapter 4

Texturation of $YBa_2Cu_3O_{7-\delta}$ tiles

4.1 Introduction

The superconducting properties of bulk melt-textured materials, especially the critical current density, depend on the growth method and on the growth conditions. In order to achieve high critical current densities two aspects are required from the processing point of view: first a matrix with well connected and orientated grains must be obtained. It is important to introduce pinning centers in the matrix in order to pin the vortices and, thus, increase the critical current densities of these materials. But these pinning centers must be homogeneously distributed in order to obtain the maximum effect of these defects. Y_2BaCuO_5 particles act as pinning centers because it has been demonstrated that their presence in YBCO matrix increases the critical current density of this superconductor [32]. One of the most common method used to achieve all these goals is melt processing.

The melt processing method has been used for the first time by Jin *et al.* [2]. The precursor sample was a mixture of Y_2O_3, $BaCuO_3$ and CuO (99.9% pure) calcinated at 895°C during 8 hours. After the calcination, the material was pressed into pellets and presintered at 925°C during 24 hours. Once the porosity is eliminated, the material is partially melt at 1100°C and, then, is slowly cooled in oxygen atmosphere until the ambient temperature is reached.

There are two kinds of peritectic reactions in this system:

1. At high temperatures above 1200°C, Y_2O_3 plus liquid (L) (L is a mixture of BaO and CuO) are stable. On cooling, these two phases react peritectically to produce Y_2BaCuO_5:

$$Y_2O_3 + L(BaO + CuO) \longrightarrow Y_2BaCuO_5 \tag{4.1}$$

2. At around 1010°C, Y_2BaCuO_5 phase reacts with liquid to produce $YBa_2Cu_3O_{7-\delta}$ phase:

$$Y_2BaCuO_5 + L(3BaCuO_2 + 2CuO) \longrightarrow 2YBa_2Cu_3O_{7-\delta} \tag{4.2}$$

By using this method YBCO samples with a low connectivity between grains and with grain boundaries with misorientation angles less than 15 degrees have been achieved. However, the critical current density values are typically between 2000 and 4000 A/cm^2 at 77K and 1T, which are too low for practical applications.

In order to improve the performances, several groups have modified this process [33, 34]: the maximum temperature of the process was decreased to the point just above the peritectic temperature of YBCO material (T_p =1010°C). Using this method, a better connectivity within the grains has been found. This method is called Melt Textured Growth (MTG) and consists of a partial melting of the material followed by a slow cooling step.

For a better understanding of the growth method and to establish the growth parameters, a phase diagram of the material is needed [1]. In figure 4.1 it is schematically represented by a pseudobinary phase diagram for YBCO material.

The YBCO system has a peritectic reaction at 1010°C as it can be seen in figure 4.1. This peritectic reaction corresponds to the descomposition of Y123 phase as follows:

$$YBa_2Cu_3O_7 \longrightarrow Y_2BaCuO_5 + L(3BaCuO_2 + 2CuO) \tag{4.3}$$

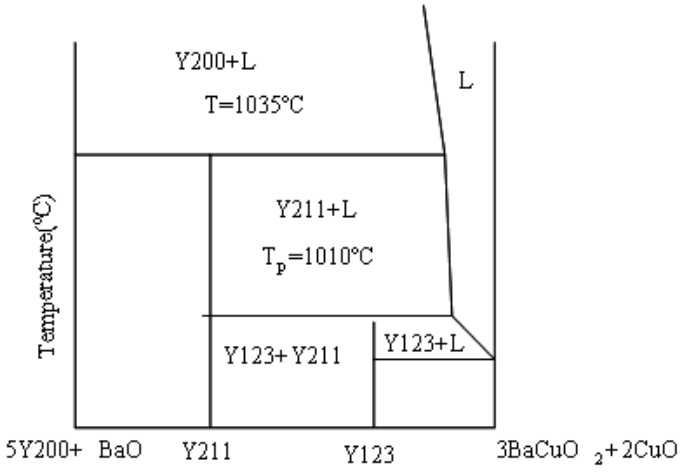

Figure 4.1: Pseudo-binary phase diagram for YBCO material

Thus, when the material is heated to a temperature above its peritectic temperature (T_p), the phase Y123 decomposes into a liquid phase and a solid one, Y211. By cooling down the semi-solid (L+S) to a temperature below the melting point of YBCO, the nucleation of Y123 starts. The solidification of YBCO starts at a temperature below the T_p, where the Y211 phase and the liquid react producing the superconducting phase Y123 through the peritectic reaction:

$$S(Y_2BaCuO_5) + L(3BaCuO_2 + 2CuO) \longrightarrow 2YBa_2Cu_3O_{6.5} \tag{4.4}$$

Melt textured materials present a large number of defects which are induced by the solidification process [1,35,36]. They are called as-grown defects and can improve or deteriorate the superconducting properties of the material. The most common defects encountered in these materials are:

1. **Microcracks and macrocracks**

   Melt textured samples, due to their high dimensions and their ceramic character have a high density of microcracks, mainly produced during the oxygen uptake process leading to the tetragonal to orthorhombic transfor-

mation. They are parallel to the ab planes, with a mean separation of the order of several μm. It has been demonstrated that Ag addition into YBCO matrix suppress the microcracks and modify their density, thus improving the superconducting quality of the YBCO samples [37].

2. **Twin boundaries**

   The similarity between the unit cell parameters a and b in the crystalline structure of $YBa_2Cu_3O_{7-\delta}$ and the transition existing between the tetragonal and orthorhombic phase at high temperatures, promote the existence of interfaces between zones having the cells parameters interchanged. These interfaces consist of two families of orthogonal planes (at 45° from the in-plane crystallographic axes) and containing the c-direction. Twin boundaries may be able to act as pinning centers [38].

3. **Non-superconducting phases**

   During the melt textured process non-superconducting phases such as Y211, $BaCuO_2$ and CuO appear and affect in one way or another the material properties. Thus, $BaCuO_2$ and CuO phases form when the reaction is incomplete and deteriorate the superconducting properties of the samples. On the contrary, Y211 particles act as pinning centers and improve the superconducting properties of the samples [39, 40]. Additionally, the existence of these particles in the YBCO matrix is very important because it has been demonstrated that they act as crack stoppers [41].

4. **Grain boundaries**

   The grain boundaries represent interfaces between two identical grains which have different orientations. They can be classified according to the misorientation angle: if the misorientation angle is less then 5°, this kind of defects are called low-angle grain boundaries and do not strongly decay the supercurrent flow. If the misorientation is more then 5° they are called

high-angle grain boundaries and act as weak links which limit drastically the supercurrent flow.

4.2 Solidification of YBCO

The crystallization process consists of disposing the atoms or molecules into an arranged solid state. This process occurs into 2 steps: first the nucleation and second the growth [42, 43].

Nucleation

During this process the atoms form clusters when they have a certain size named critical radius r^*. There are two types of nucleation: homogeneous and heterogeneous nucleations. The homogeneous nucleation is spontaneous and the atoms from the liquid phase form the nucleus at the solid state. On the contrary, the heterogeneous nucleation is stimulated by the presence of grain boundaries, impurity particles, defects existent in the crystal or interfaces.

Crystal growth

After the nucleation, the crystal growth takes place. In this step the liquid phase is totally eliminated.

In homogeneous nucleation it is assumes that the system is free from impurities. Creation of particles as a new phase, as a nucleus, is associated with a change in the free energy of the system. The change in energy is caused by two factors:

1. generation of volume of the new phase (ΔG_V);
2. creation of an interface due to the increasing size of nucleus (ΔG_S).

Thus:

$$\Delta G = \Delta G_V + \Delta G_S \tag{4.5}$$

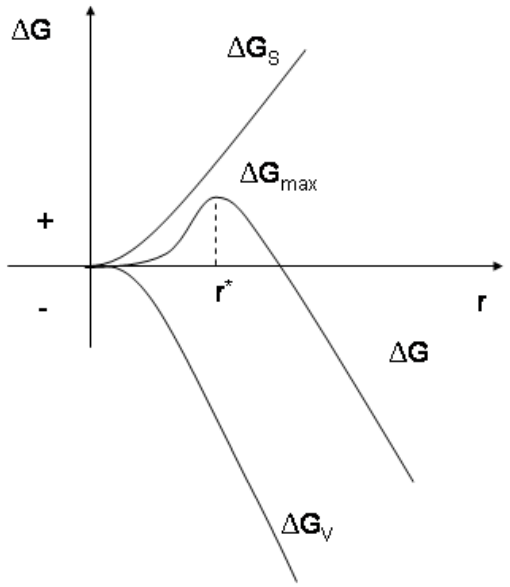

Figure 4.2: Change in the free energy ΔG and its components during the formation of a nucleus [42]

In figure 4.2 it is represented the change in free energy and its components during the formation of a nucleus. It can be observed that the change in the free energy associated with the increasing volume of a nucleus, ΔG_V, is always negative because the transition occurs from an unstable to a stable state and is proportional to r^3. On the contrary, the change in free energy due to the generation of the interface surface of the developing nucleus is always positive and it is proportional to r^2. It may be seen from figure 4.2 that the free energy change increases with r until a maximum value corresponding to a certain critical value, r^*. When the radius is lower then the critical value, $r < r^*$, the nucleus is unstable and dissociates because its growth leads to an increase in the total free energy change, ΔG. However, when $r > r^*$, the nucleus can grow further because further growth leads to a decrease in the total free energy change. At the maximum value of ΔG the nuclei is stable.

For the YBCO system, at its peritectic temperature, there exists an equilib-

rium between the solid and liquid phases:

$$S1(Y211) + L \longleftrightarrow S2(Y123) \tag{4.6}$$

This means that the free energy change G_{S1+L} is equal to the G_{S2}. When the liquid phase is stable, the variation in the free energy will be maximum when the radius of the nucleus reaches the critical size r^*.

For the solidification solid clusters must exist in the liquid and the variation in free energy must be negative (see equation 4.7). This will happen when the temperature is lower than the peritectic temperature of the YBCO system (T_p).

$$\Delta G = (G_{S1+L} - G_{S2}) < 0 \tag{4.7}$$

Cima *et al.* [44] and Izumi *et al.* [45] have developed a model to explain the mechanism of Y123-growth. They demonstrate that Y123 does not nucleate around the Y211 phase but in the eutectic liquid (L). The yttrium required to solidify Y123 is provided by the Y211 dissolution followed by the yttrium diffusion, through the liquid, to the Y123/L interface. In the model developed by Cima *et al.* it is supposed that the Y211 particles are dissolved partially before the growth front. To explain the yttrium diffusion we consider that C_{L-123} is the concentration of yttrium in the liquid at the Y123/L interface, C_{L-211} is the metastable concentration of yttrium far from the growth front and nearby the Y211 particle. C_{L-211} being higher than C_{L-123}, creates a gradient in the yttrium concentration and a transport of this appears to the growth front. In this way the concentration of yttrium nearby a Y211 particle decreases. To maintain a metastable composition of C_{L-211}, the Y211 particles are dissolved in the liquid, thus continuing the migration of yttrium to the growth front and being possible the continuous growth of Y123 phase.

Assuming this growth mechanism, Cima *et al.* have developed a model where the growth rate, R, for plane front solidification, can be written as in the equation

4.8.

$$R(C_{S123} - C_{L123}) = \frac{D_L}{l}(C_{L211} - C_{L123}) \tag{4.8}$$

where D_L is the diffusion constant of yttrium through liquid, C_{S123} is the yttrium concentration in Y123 phase, C_{L123} is the yttrium concentration in the liquid at the interface liquid/solid and l is the distance between a Y211 particle and the Y123 interface.

Y211 particles continue dissolving until they are trapped by the growth front and included in the Y123 matrix if they are large and pushed by growth front if their size is small [46].

4.3 Generation of YBCO monodomains

Since the initiation of melt processing, significant progress has been achieved in the development of melt-texturing methods. These various methods can be classified into four categories, namely:

1. slow-cooling without an imposed temperature gradient
2. slow-cooling in the presence of temperature gradient but without sample transport;
3. slow cooling in a temperature gradient with sample transport;
4. seeding.

Besides these major types of melt-texturing method, modifications in the sample stoichiometry, the type of precursor sample, the addition of secondary phases are also used. Each of these methods and its modifications affect the final microstructure, thus the superconducting properties of the melt-textured samples.

The melt-textured methods that belong to the first two categories are essentially non-directional processes and the resulting superconductors consist

of multiple-orientated domains. The boundaries separating these domains are high-angle boundaries, which frequently contain secondary phases. Thus, the superconducting properties of these samples are rather poor.

The latter two categories are directional melt-texturing processes and the most common methods from this category used to grow YBCO monoliths are:

1. *Bridgmann Growth*: in this case, the mixture is compressed (under isostatic pressure) as a bar. The main characteristic of this method is the use of a furnace with a gradient of temperature so that the maximum temperature obtained is slightly higher than the peritectic temperature of the mixture. The bar is placed in this furnace and slowly moved upwards. A region of the bar, the one placed on the hottest region of the furnace, is found to be in the melt state (the large viscosity of the mixture, even in the liquid state, avoids the bar from falling). As the liquid region of the bar is moved away from the zone with a maximum temperature, it starts to solidify. Different grains appear at the beginning of this process, but the different growth rate between them promotes the existence of a single grain. After this initial competition, the remaining grain induces the oriented solidification of the liquid [47, 48].

2. *Top Seeding melt textured growth*. It consists of controlling the nucleation sites and the crystal growth orientation by using a seed placed on the top of the sintered sample before texturation [49, 50].

In this thesis, we have used samples obtained by the Top Seeding Melt Textured Growth Method. Some of the samples used in this PhD thesis have been obtained in ICMAB and some of them were supplied by IPHT Jena Laboratory and Nexans Superconductors.

4.4 Top Seeding Melt Textured Growth

The Top Seeding Melt Textured Growth method (TSMG) is widely used to obtain Y123 monoliths with high critical current densities. A seed is placed on the top of the sample in order to act as a nucleation center. A material, to be used as seed must accomplish two conditions: first, a peritectic temperature higher that the material to be textured thus remaining in a solid form when Y123 is heated past its peritectic temperature; and second the material must have similar crystallographic parameters as the YBCO matrix.

The most common materials considered effective as seeds are Sm123 and Nd123. The use of a seed allows to act principally in a given temperature range named the solidification window. This window is linked with the temperatures of heterogeneous and homogeneous nucleation. The heterogeneous nucleation from the seed takes place at a higher temperature than the homogeneous nucleation.

Once the heterogeneous nucleation has taken place, the grain grows due to the Y diffusion from the Y211 particles towards the growth front. At the highest temperature of the window, the diffusion is fast and the nuclei has no difficulty to grow. However, at lower temperatures, several phenomena take place and affect the growth and the homogeneity of the domain. One of them is the pushing/trapping phenomena [51]. For an homogeneous distribution of the Y211 particles into the YBCO matrix, they must have a radio r_c (4.9) [52], named critical radius and whose formula is:

$$r_c \sim \frac{\Delta\sigma \cdot a_0}{3 \cdot \eta \cdot R} \tag{4.9}$$

where $\Delta\sigma = \sigma_{PS} - \sigma_{PL} - \sigma_{SL}$ and $\sigma_{PS,SL,PL}$ are the interface free energies from the particle-solid, solid-liquid and particle liquid, respectively whereas R is the solidification growth rate, σ is the liquid viscosity and a_0 is the average intermolecular distance.

It has has been observed that if the radius of Y211 particles is below r_c, the particles are pushed toward the Y123/L front. On the contrary, if the radius of the Y211 particles is larger than r_c, these particles are trapped into the YBCO matrix. In these cases an inhomogeneous distribution of Y211 particles is obtained, thus a reduction of the critical current density can occurs.

The TSMG method can be used to obtain high-T_c superconductors with high critical currents but their dimension cannot exceed 4 cm. One of the difficulties is due to the competition between the growth of the grain from the seed (heterogeneous nucleation) and the growth of different grains from the liquid (homogeneous nucleation). Thus, a detailed understanding of the mechanism of this process is needed in order to avoid homogeneous nucleation and finalize the texturation with one single grain grown from the seed and therefore with a single orientation.

4.5 Preparation of $YBa_2Cu_3O_{7-\delta}$ monodomains

The initial YBCO samples used in this PhD thesis for joining have been supplied by IPHT Jena and Nexans Superconductors. As well, we have used samples obtained in ICMAB laboratory. All the samples used have been obtained by Top-Seeding Melt-Textured Growth method. The precursors for the melt-texturing process were supplied by Hoechst and the Solvay Barium Strontium. The samples provided by Nexans Superconductors were square shaped with dimensions of 40mm×40mm×14mm and possessed a composition of Y123+25mol%Y_2O_3+1%CeO_2 [53], whereas the samples supplied by IPHT Jena have a composition of $Y_{1.5}Ba_2Cu_3O_{7-\delta}$ with 1%wtCeO_2 addition prepared by mixing the Y123 powders, Y_2O_3 and CeO_2 [54]. A mixture of commercial powder of the Y123 phase from Solvay and the Y211 phase from Praxair has been used to obtain the samples in ICMAB. The composition used was $69\%wtY123 + 30\%wtY211 + 1\%wtCeO_2$. The difference between the methods used for growth of YBCO monoliths is that IPHT Jena and Nexans Superconductors have optimized

their process for batch productions, whereas the process used in ICMAB permits the obtention of YBCO monoliths in small dimensions (cylinders of 12mm in diameter). In the section to follow will be presented the process used to obtain YBCO monoliths in ICMAB.

ICMAB process

The Y123 phase is the superconducting phase and the Y211 phase is the non-superconducting one. The effect of Y211 addition to the YBCO matrix is to:

- diminish the size of Y211 particles provided from the peritectic decomposition of Y123 phase [55];
- prevent losses of liquid during the melting;
- act as pinning centers for the vortices when are trapped in the textured Y123 [32]. In this way the critical current density of the material (J_c) is improved;
- act as crack stoppers, thus improving the mechanical properties of the samples.

Additionally, by introducing CeO_2 particles to the YBCO matrix, it has been found that: first, these particles increase the number of the nucleation centers for the Y211 particles created during the peritectic decomposition. For instance, the size of these particles is reduced [56]. And second, the existence of these particles in the YBCO matrix increase the viscosity of the liquid in the semi-solid state [57] and, as a consequence, liquid losses are avoided during the high-temperature process.

Once the composition is mixed, the powder is pressed into cylindrical pellets with a diameter of 12mm and the hight of 10mm (see figure 4.3). The pellets are pressed using an uniaxial prense SPECAC which can use pressure until 25000 bars. For the samples used for joining, we have applied a pressure of 3000 bars; a higher pressure could fracture the sample or could generate microcracks or

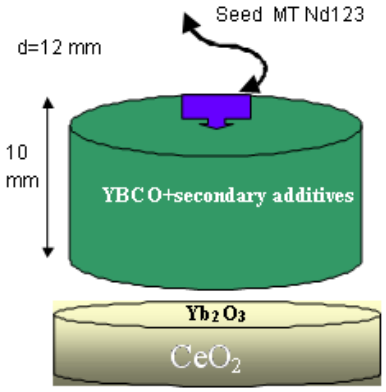

Figure 4.3: The configuration used to obtain YBCO monoliths: a Nd123 seed is situated on the top of the YBCO pellet. The compacted powder is located on a support consisting of Yb_2O_3 and CeO_2

macrocracks. For controlling the orientation of the single-domain, the seed is located on the top of the pellet before texturing. To induce the growth parallel to the ab plane, the Nd123 seed is situated with its ab plane in contact with the surface of the YBCO pellet.

For a better growth, the best contact between the seed and the sample is necessary. The pellet is located on a support of Yb_2O_3 and CeO_2 in order to avoid the liquid losses and the contamination of the material (see figure 4.3). By heating the sample to a high temperature a reactive liquid is formed. Thus, it is important to find a support to avoid at the same time the contamination of the sample with the material which it is made of, liquid losses and germination of crystals at the interface sample/support. For instance, we need a material of high purity and high melting temperature. As a consequence, a ceramic of CeO_2 is introduced to avoid the liquid losses and the reaction of the sample with the alumina block during the thermal process. Moreover, in order to avoid the formation of irregular nucleations at the bottom of the sample, we have covered the CeO_2 with a thin film of Yb_2O_3 powder. The formation of such irregular nucleations could reduce the size of the single domain of the YBCO monolith.

As it was mentioned before, the material, to be used as support during the thermal treatments must has a peritectic temperature lower than the melting point of the YBCO material and, consequently, lower than that of the seed. Thus, at the highest temperature of the profile Yb_2O_3 reacts with the liquid L($BaCuO_2$+CuO) as follows:

$$Yb_2O_3 + L(BaCuO_2 + CuO) \longrightarrow Yb211(solid) + L \tag{4.10}$$

Lately, the Yb211 phase can react with the liquid according to a similar reaction with 4.4 resulting the Yb123 phase. The Yb123 peritectic temperature is lower than the solidification temperature of YBCO. In this way, during the solidification window of Y123 phase, the inferior interface sample/support is in a liquid state and does not promote any nucleation of Y123.

In figure 4.4 it is represented the temperature profile to which the YBCO samples have been subjected at ICMAB.

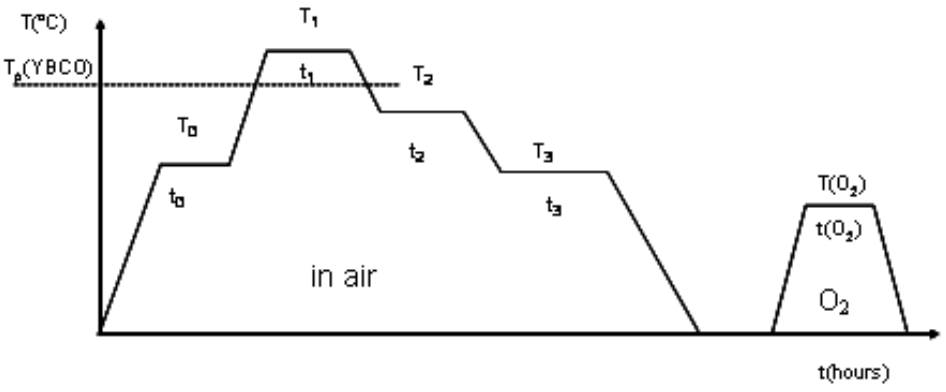

Figure 4.4: Temperature profile to which the YBCO pellets have been subjected: the texturation has been done in air and the superconducting behavior of the sample has been restablished by oxygenation.

The YBCO system has the peritectic temperature at T_p =1010°C. To obtain an homogeneous material, the Y211 phase should be distributed homogeneously in

the YBCO matrix. Thus, the Y123 and Y211 phases are first mixed and ground. For a better compactation, the sample is subjected to a presintering process consisting of heating the sample to a temperature T_0=963°C during t_0=40 hours. During this process the residual porosity is reduced or eliminated. The pellet is overheated to T_1=1035°C during t_1=4 hours. At this temperature the Y123 material melts completely, while the Nd123 seed [58] is kept in a solid state. Soon after, the sample is cooled down rapidly with a cooling rate of 200°C/h until a temperature T_2=1008°C is reached. Starting with this temperature, which is slightly above the peritectic temperature of YBCO, enables the heterogeneous nucleation from the seed begin. Thus, the heterogeneous growth from the seed takes place between the temperatures T_2 y T_3. For a plane crystal growth the sample must be cooled down slowly. Thus we have used a cooling rate of 0.2°C/h and the temperature T_3 is 990°C. Starting with this temperature T_3 the homogenous nucleation should begin. But, using this profile we have already grown all the crystal before reaching this temperature, so this nucleation was avoided. Finally, the sample is cooled down rapidly until the ambient temperature is reached. This texturing process has been done in air. Now, to reestablish the superconducting behavior of the YBCO sample, the pellet is subjected to another thermal treatment but in oxygen atmosphere. The maximum temperature and the time needed for a full oxygenation depend on the dimensions of the sample. The optimal oxygenation treatment for samples with a diameter of 12mm and height of 10 mm is of 120 hours under a pressure of 1atm and at T_{ox}=450°C [58], [57].

The samples provided by Jena and Nexans Superconductors were obtained employing a similar process of TSMG as that used in ICMAB and exhibit similar superconducting properties. The difference with the process used in ICMAB was that their process is scaled-up for industrial application. With the aim to weld YBCO monoliths supplied by IPHT Jena and Nexans Superconductors, we had to eliminate 0.8cm from the bottom part of the samples because they display a large amount of porosity, Y211 particles and macrocracks which could affect the

microstructure and superconducting properties of the final joints.